Earth and Planetary Science Letters 443 (2016) 81–89

Contents lists available at ScienceDirect

Earth and Planetary Science Letters

www.elsevier.com/locate/epsl

Influence of organics and silica on Fe(II) oxidation rates and cell–mineral aggregate formation by the green-sulfur Fe(II)-oxidizing bacterium *Chlorobium ferrooxidans* KoFox – Implications for Fe(II) oxidation in ancient oceans

Tina Gauger [a], James M. Byrne [a], Kurt O. Konhauser [b], Martin Obst [c], Sean Crowe [d], Andreas Kappler [a,*]

[a] Geomicrobiology, Center for Applied Geosciences, University of Tuebingen, 72076 Tuebingen, Germany
[b] Department of Earth and Atmospheric Sciences, University of Alberta, Edmonton, Alberta T6G 2E3, Canada
[c] Environmental Analytical Microscopy, Center for Applied Geosciences, University of Tuebingen, 72076 Tuebingen, Germany
[d] Department of Microbiology and Immunology and Department of Earth, Ocean, and Atmospheric Sciences, University of British Columbia, V6T 1Z3 Vancouver, Canada

ARTICLE INFO

Article history:
Received 3 December 2015
Received in revised form 10 March 2016
Accepted 12 March 2016
Available online xxxx
Editor: D. Vance

Keywords:
Fe(II) oxidation
green sulfur bacteria
cell–mineral aggregates

ABSTRACT

Most studies on microbial phototrophic Fe(II) oxidation (photoferrotrophy) have focused on purple bacteria, but recent evidence points to the importance of green-sulfur bacteria (GSB). Their recovery from modern ferruginous environments suggests that these photoferrotrophs can offer insights into how their ancient counterparts grew in Archean oceans at the time of banded iron formation (BIF) deposition. It is unknown, however, how Fe(II) oxidation rates, cell–mineral aggregate formation, and Fe-mineralogy vary under environmental conditions reminiscent of the geological past. To address this, we studied the Fe(II)-oxidizer *Chlorobium ferrooxidans* KoFox, a GSB living in co-culture with the heterotrophic *Geospirillum* strain KoFum. We investigated the mineralogy of Fe(III) metabolic products at low/high light intensity, and in the presence of dissolved silica and/or fumarate. Silica and fumarate influenced the crystallinity and particle size of the produced Fe(III) minerals. The presence of silica also enhanced Fe(II) oxidation rates, especially at high light intensities, potentially by lowering Fe(II)-toxicity to the cells. Electron microscopic imaging showed no encrustation of either KoFox or KoFum cells with Fe(III)-minerals, though weak associations were observed suggesting co-sedimentation of Fe(III) with at least some biomass via these aggregates, which could support diagenetic Fe(III)-reduction. Given that GSB are presumably one of the most ancient photosynthetic organisms, and pre-date cyanobacteria, our findings, on the one hand, strengthen arguments for photoferrotrophic activity as a likely mechanism for BIF deposition on a predominantly anoxic early Earth, but, on the other hand, also suggest that preservation of remnants of Fe(II)-oxidizing GSB as microfossils in the rock record is unlikely.

1. Introduction

Geochemical conditions of the Precambrian oceans were different from today, with dissolved silica concentrations at least 1 mM (Jones et al., 2015), and potentially approaching the saturation state of amorphous silica (up to 2.2 mM) (Siever, 1962), while dissolved Fe(II) concentrations ranged from 50 µM (Holland, 1973) to ~1 mM (Morris, 1993). Under these siliceous and ferruginous conditions the deposition of banded iron formations (BIF) took place (see Bekker et al., 2014 for review). Several mechanisms have been put forth to explain Fe(II) oxidation in Precambrian oceans: (1) abiotic or microbiological reactions with O_2 produced by cyanobacteria, (2) abiotic, UV-induced photo-oxidation, or (3) direct photosynthetic utilization of Fe(II) by phototrophic Fe(II)-oxidizers, the so called photoferrotrophs. Emerging evidence suggests that photoferrotrophs were the most probable drivers for the deposition of the precursor ferric oxyhydroxide layers that led to BIF before the Great Oxidation Event, some 2.45 billion years ago (Czaja et al., 2013; Kappler et al., 2005).

* Corresponding author at: Geomicrobiology, Center for Applied Geosciences, University of Tuebingen, Sigwartstrasse 10, D-72076 Tuebingen, Germany. Tel.: +49 7071 2974992; fax: +49 7071 29 295059.
E-mail address: andreas.kappler@uni-tuebingen.de (A. Kappler).

http://dx.doi.org/10.1016/j.epsl.2016.03.022
0012-821X/

Photoferrotrophic organisms use light energy and Fe(II) as an electron donor for CO_2 reduction and the production of cell biomass (Widdel et al., 1993). This type of metabolism was shown to be widespread amongst freshwater and marine phototrophic bacteria, including purple sulfur bacteria (Croal et al., 2004), purple non-sulfur bacteria (Poulain and Newman, 2009; Widdel et al., 1993; Wu et al., 2014) and green sulfur bacteria (GSB) (Crowe et al., 2008; Heising et al., 1999). To date, the bulk of our understanding on how photoferrotrophs metabolize, and under what environmental conditions, has mainly come from the study of purple non-sulfur bacteria. However, it has been shown that in modern ferruginous freshwater lakes, GSB were present in the anoxic layers of the photic zone, where they can play an important role for the biogeochemical Fe and C cycles in these environments (Crowe et al., 2008; Llirós et al., 2015). Due to their adaptation to low light conditions (Llirós et al., 2015), GSB are perfectly suited for such conditions, much better than purple-sulfur and purple non-sulfur bacteria, underpinning their importance in ferruginous environments.

Only one strain of GSB capable of phototrophic Fe(II) oxidation has been studied in detail (Heising et al., 1999). This *Chlorobium ferrooxidans* strain KoFox was shown to oxidize Fe(II) at very low light intensities (>50 lux) (Hegler et al., 2008). It also grows in co-culture with *Geospirillum* sp. strain KoFum; the latter grows by fermenting fumarate to organic acids, which in turn, enhances Fe(II) oxidation by KoFox (Heising et al., 1999). It is known from abiotic Fe(II) oxidation experiments that the presence of such organics during Fe(II) oxidation influences the structure, particle size, and crystallinity of Fe(III) minerals (Mikutta et al., 2008).

Previous studies have additionally revealed that in the Fe(II)-oxidizing co-culture KoFox/KoFum, the cell surfaces of the fermenting strain KoFum become thinly encrusted in Fe(III) minerals after Fe(II) oxidation. In contrast, cells of the Fe(II)-oxidizing KoFox remained largely free of Fe(III) particles, with the exception of sparse, flat mineral particles (Schädler et al., 2009). This suggests that in this co-culture it is probably the non-Fe(II)-oxidizing partner and not the Fe(II)-oxidizer that will leave a trace in the rock record as a mineral-encrusted microfossil. However, these previous biomineralization studies have not taken into account the complex chemistry of ancient seawater, and how the presence of organic compounds consumed and produced by KoFum influences the mineralogy of the resulting ferric oxyhydroxides, or the influence that different activities of the Fe(II)-oxidizer might have on encrustation. For instance, dissolved silica has a high affinity for iron and it can influence the association of the cells with Fe(III) minerals (Eickhoff et al., 2014; Mayer and Jarrell, 1996). As the Precambrian oceans were Si-rich, its presence might have influenced cell–mineral interactions and thereby needs to be considered when conducting such experiments.

This study, therefore, aims to answer the following questions: (i) how do dissolved silica, fumarate (as an organic model compound that is fermented by KoFum), and variable light intensities impact the activity of the Fe(II)-oxidizer and thus influence Fe(II) oxidation rates, encrustation patterns and cell–mineral interactions in the KoFox/KoFum co-culture, and (ii) which minerals are formed during Fe(II) oxidation in the presence and absence of dissolved silica and organics.

2. Methods

2.1. Source of microorganisms

Chlorobium ferrooxidans strain KoFox was described as the first GSB capable of using Fe(II) as electron donor coupled to anoxygenic photosynthesis (Heising et al., 1999). It grows in co-culture with the fermenting ε-proteobacterium *Geospirillum* sp. strain KoFum. The co-culture was isolated from a ditch at the University of Konstanz, Germany (Heising et al., 1999), and provided by B. Schink (University of Konstanz, Germany). It has been maintained in our lab strain collection since.

2.2. Microbial growth medium and growth conditions

For routine cultivation, the co-culture was grown in 22 mM bicarbonate-buffered mineral medium (pH 7), which was prepared anoxically, as previously described by Hegler et al. (2008). The Fe(II)-containing medium was sterile filtered in an anoxic chamber with a 0.22-mm filter (polyethersulfone, Millipore) 48 h after the $FeCl_2$ solution was added and Fe(II) minerals precipitated. Final concentration of dissolved Fe(II) in the medium after filtration was ~3–4 mM. In cultivation experiments with dissolved silica present, 2 mM $Na_2SiO_3 \times 9\ H_2O$ was added just before inoculation. For enhanced growth of both strains, 5 mM sodium fumarate was added to some experiments. In cultures grown without Fe(II) as an electron donor, a few % of hydrogen gas was added to the headspace (20:80 N_2/CO_2) with a sterile syringe as alternative electron donor. For growth experiments, serum bottles with 25 mL Fe(II)-containing mineral medium were inoculated with 10% of the co-culture grown on H_2 and incubated at 20 °C with either high (~1300 lux), moderate (~450 lux) or low (~25 lux) light conditions until all Fe(II) was oxidized. Based on daylight attenuation data of pure ocean water for a wavelength of 465 nm, that lies within the main absorption wavelength range of GSB carotenoids, the high, moderate, and low light conditions represent a depth of approximately ~80 m, ~100 m, and >160 m in the marine photic zone, respectively (Jerlov, 1976). For more turbid water, high, moderate, and low light conditions represent a depth of approximately ~35 m, ~50 m, and >80 m (Jerlov, 1976).

2.3. Analytical methods

Iron was quantified with the spectrophotometric ferrozine assay. Briefly, 100 µl of culture suspension was withdrawn anoxically with a syringe and stabilized in 900 µl of 1 M HCl. The purple ferrozine-Fe(II) complex was quantified at 562 nm using a microtiter plate reader (SpectraMax M2, Molecular Devices, USA, and Multiskan™ GO, Thermo Fisher Scientific, USA). Ferrozine measurements were done in triplicate. Maximum rates of microbial Fe(II) oxidation were calculated for each culture vial from the steepest slope between two subsequent data points of Fe(II) concentrations. Fe(II) oxidation rates are presented as mean ± SD (standard deviation) and an unpaired, two-tailed *t*-test was used to determine whether the Fe(II) oxidation rates obtained in the presence of Si were statistically significant from the average value obtained in absence of Si (Fig. 2).

Fumarate and other organic acids were quantified by high performance liquid chromatography (Bio Rad Aminex HPX-87H Ion Exclusion Column and 5 mM H_2SO_4 eluent).

2.4. Electron microscopy

For scanning electron microscopy (SEM), samples were taken at different time intervals during Fe(II) oxidation. Similar to the sample preparation described earlier (Schädler et al., 2009), 1 mL of a culture was taken with a sterile syringe that had been flushed with N_2. Samples were then centrifuged (5 min at 5000 × g), the supernatant removed, and the pellet resuspended in 1 mL fixative (2.5% glutaraldehyde, 2% paraformaldehyde in 0.1 M phosphate buffer) overnight at 4 °C. To remove the fixative, samples were centrifuged again (5 min at 5000 × g), the supernatant was discarded, the pellet was resuspended in 50 µL of 0.1 M phosphate buffer, and

then a small aliquot was pipetted on carbon-coated TEM grids. The samples were washed twice with 0.1 M phosphate buffer and successively dehydrated using a series of ethanol dilutions (30, 50, 70, 90, and twice 100%). Instead of critical point drying (CPD), the samples were dried with hexamethyldisilazane (HMDS). Dried samples were mounted on aluminum stubs using double-sided carbon tape and coated in a Leica EM SCD005 evaporative carbon coater with a thin layer of carbon. Imaging was performed with a JEOL 6301F (Field Emission Scanning Electron Microscopy [FESEM]) operating at 5 kV at the Department of Earth and Atmospheric Sciences, University of Alberta, and a LEO 1450 VP operating at 12 kV (SE and BSE) using an Everhard–Thornley and a backscattered electron detector at the Center for Applied Geoscience, University of Tuebingen.

For transmission electron microscopy (TEM), samples were taken at the late exponential growth phase when Fe(II) was completely oxidized. Fixed samples were washed three times with 0.1 M phosphate buffer, post-fixed with 1% osmium tetroxide in 0.1 M phosphate buffer for 1 h and washed again three times with 0.1 M phosphate buffer. Dehydration of the samples was achieved with a graded ethanol series (50, 70, 90, and 3 times 100%). Subsequently, samples were infiltrated with 50% Spurr resin in ethanol for 3 h twice, 100% Spurr resin overnight and 100% Spurr resin for 3 h twice the next day. After that, samples were embedded in flat molds with fresh Spurr resin and hardened in an oven at 70 °C overnight. TEM sectioning was performed with an Ultra-microtome (Reichert UltraCut E, Austria) using a glass knife. Ultrathin sections with 90 to 110 nm thickness were then placed on carbon-coated copper TEM grids. Before imaging, samples were post-stained with uranyl acetate and then lead citrate. TEM images were acquired using a Philips/FEI Morgagni 268 TEM with Gatan Digital Camera and operated at 80 kV at the University of Alberta.

2.5. Mineral analysis

Samples for mineral analysis were taken at the end of each experiment after Fe(II) oxidation was completed. Sampling was conducted in an anoxic chamber (90% N_2/10% H_2) to avoid the formation of secondary Fe(III) minerals. 10–20 mL sample were taken with a sterile syringe and filtered onto cellulose filters (0.45 µm, Millipore).

For ^{57}Fe Mössbauer spectroscopy at 77 K and 5 K, filter papers were sealed between two layers of oxygen-impermeable adhesive polyimide tape (Kapton) and stored anoxically at −20 °C. Samples were loaded into a closed cycle exchange gas cryostat. The Mössbauer spectrometer (WissEL) in the Geomicrobiology group at the University of Tuebingen, Center for Applied Geosciences, was operated in transmission mode, with a ^{57}Co/Rh source driven in constant acceleration mode. The Mössbauer spectrometer instrument was calibrated with a 7 µm thick α-^{57}Fe foil measured at room temperature, which was also used to determine the half width at half maximum (fixed to 0.146 mm/s during fitting). Fitting was carried out using Recoil (University of Ottawa) with the Voigt based fitting routine (VBF) used for 77 K spectra and the extended Voigt based fitting routine (xVBF) used for 5 K spectra (Lagarec and Rancourt, 1997).

For µ-XRD (X-ray diffraction) analysis, sample filters were stored anoxically in Eppendorf vials at −20 °C. Samples were then dried in an anoxic chamber (100% N_2), homogenized, mounted onto a Si single crystal silicon wafer and subsequently examined with a Bruker D8 Discover GADDS XRD^2-microdiffractometer (Bruker AXS GmbH, Germany) equipped with a Co Kα X-ray tube and a 2-dimensional HI-STAR-detector operating at 30 kV/30 mA. To identify the containing mineral phases, EVAR® 10.0.1.0 software and the PDF-database licensed by ICDD (International Centre for Diffraction Data) were used.

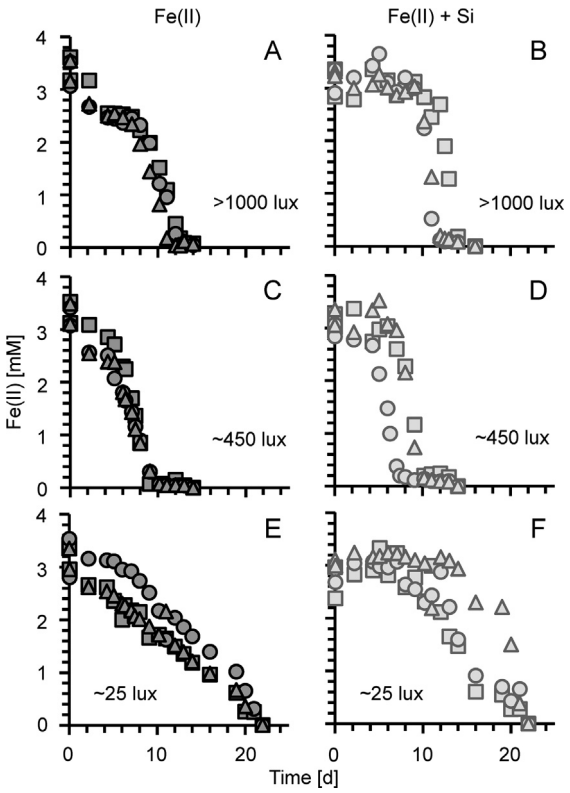

Fig. 1. Fe(II) oxidation rates of *Chlorobium ferrooxidans* strain KoFox in co-culture with *Geospirillum* sp. strain KoFum over time grown with ~3 mM Fe(II) (A, C, E) or ~3 mM Fe(II) and ~2 mM dissolved silica (B, D, F) either under high light conditions (~1300 lux; A+B), normal light (~450 lux; C+D) or low light (~25 lux; E+F). The three different symbols (triangles, circles and squares) correspond to triplicate cultures.

3. Results

3.1. Fe(II) oxidation rates at different light intensities and in presence of silica

To determine the influence of dissolved silica and different light intensities on Fe(II) oxidation rates of KoFox, the co-culture was grown under high (~1300 lux), moderate (~450 lux) and low (~25 lux) light conditions, either in the absence or presence of dissolved silica. Fe(II) oxidation under high light conditions started after a delay of approximately 9–10 days in the absence (Fig. 1A) or presence (Fig. 1B) of dissolved silica, but was significantly faster when silica was present (1.66 ± 0.34 mM/day vs. 0.71 ± 0.06 mM/day).

Under moderate and low light conditions almost no delay in Fe(II) oxidation was observed, i.e., Fe(II) oxidation started shortly after inoculation. Fe(II) oxidation rates were 0.82 ± 0.07 mM/day at moderate and 0.59 ± 0.10 mM/day at low light, respectively, when cultures were solely grown on Fe(II) (Fig. 1 C+E). In the presence of dissolved silica Fe(II) oxidation rates were, similar to the high-light conditions, also faster with 1.32 ± 0.26 mM/day at moderate and 0.89 ± 0.19 mM/day at low light, respectively (Fig. 1 D+F). In summary, our data shows that Fe(II) oxidation rates in the presence of dissolved silica showed the highest rates at the highest light intensities and decreased with decreasing light intensities from 1.66 ± 0.34 mM/day at high light to 1.32 ± 0.26 mM/day at moderate to 0.89 ± 0.19 mM/day at low light while cultures grown without dissolved silica showed highest Fe(II) oxidation rates of 0.82 ± 0.07 mM/day at moderate light intensities (Fig. 2).

The addition of fumarate had an ambiguous effect on the Fe(II) oxidation rates: at low light conditions Fe(II) oxidation in the pres-

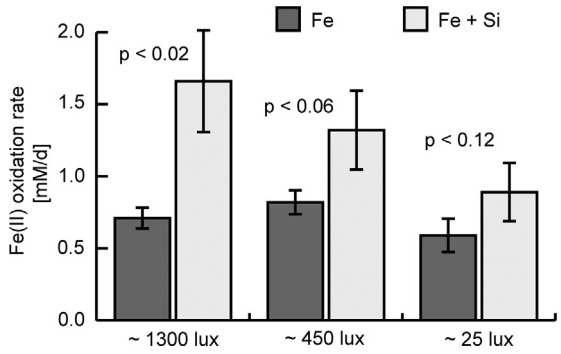

Fig. 2. Fe(II) oxidation rates of *Chlorobium ferrooxidans* KoFox in co-culture with *Geospirillum* sp. KoFum, either grown with ~3 mM Fe(II) (dark grey) or with ~3 mM Fe(II) and 2 mM silica (light grey) at different light intensities (high light = ~1300 lux, normal light = 450 lux, low light = 25 lux); Rates were calculated from steepest slopes of every triplicate culture and *p* values calculated with 2-tailed *t*-test. Error bars indicate standard deviation calculated from three parallels.

ence of silica was slightly enhanced by fumarate addition from 0.85 ± 0.06 mM/day in its absence to 1.57 ± 0.63 mM/day in its presence (data not shown). At moderate light conditions Fe(II) oxidation decreased from 1.44 ± 0.39 mM/day in its absence to 0.63 ± 0.25 mM/day in its presence (in the presence of silica from 1.97 ± 0.18 mM/day to 0.71 ± 0.20 mM/day). Surprisingly, Fe(II) oxidation in the presence of fumarate stopped after 10–12 days, and a slight reduction in Fe(III) of ca. 0.16 ± 0.02 mM/day and ca. 0.29 ± 0.06 mM/day was observed in the presence of silica in some experiments (data not shown).

3.2. Cell–mineral aggregate in the Fe(II)-oxidizing co-culture KoFox/KoFum

To investigate cell–mineral aggregate in the KoFox/KoFum co-culture, FESEM was used to image the cells at different time intervals during Fe(II) oxidation. Both strains have different cell morphologies and sizes which allowed us to easily distinguish between them: KoFum cells are elongated and slightly thicker than the small and oval-shaped KoFox cells when grown on H_2 (Fig. 3A), but also in cultures grown on Fe(II) (Fig. 3B). FESEM imaging of samples at the end of Fe(II) oxidation further revealed mineral precipitates on some cell surfaces, but a distinct encrustation pattern for either one of the two strains was not observed (Fig. 3 B–G). Mineral precipitates in the presence of silica had more globular structures (Fig. 3G) as compared to the spiky-shaped Fe(III) minerals in samples without silica present (Fig. 3F). The same mineral morphology and cell–mineral aggregation patterns were observed in samples analyzed from earlier time intervals (data not shown).

To distinguish between iron and organic precipitates on the cell surfaces, secondary electron (SE) as well as backscattered electron (BSE) imaging on the SEM was used. In BSE mode, iron exhibits a much stronger signal than carbon due to its higher atomic number, which makes it possible to visualize iron encrustation. In our samples, iron precipitates inside the cells or at the cell surfaces were not observed in BSE mode and the cells appeared less bright, i.e. less visible, (Fig. 4) compared to SE mode.

To further evaluate the possibility of cell surface precipitations, TEM was conducted with samples of the co-culture grown on H_2 (Fig. 5A) compared to samples of the co-culture grown with Fe(II) (Fig. 5 B+D) or with Fe(II) and silica (Fig. 5 C+E) at the end of Fe(II) oxidation. In contrast to SEM, this method can be used to visualize the internal cell structure. We observed that the mineral precipitates similarly showed needle-like, spiky structures with rough surfaces for samples grown with Fe(II) (Fig. 5 B+D) compared to globular (i.e., spherical) mineral structures with smooth surfaces in samples where silica was present (Fig. 5 C+E). Some

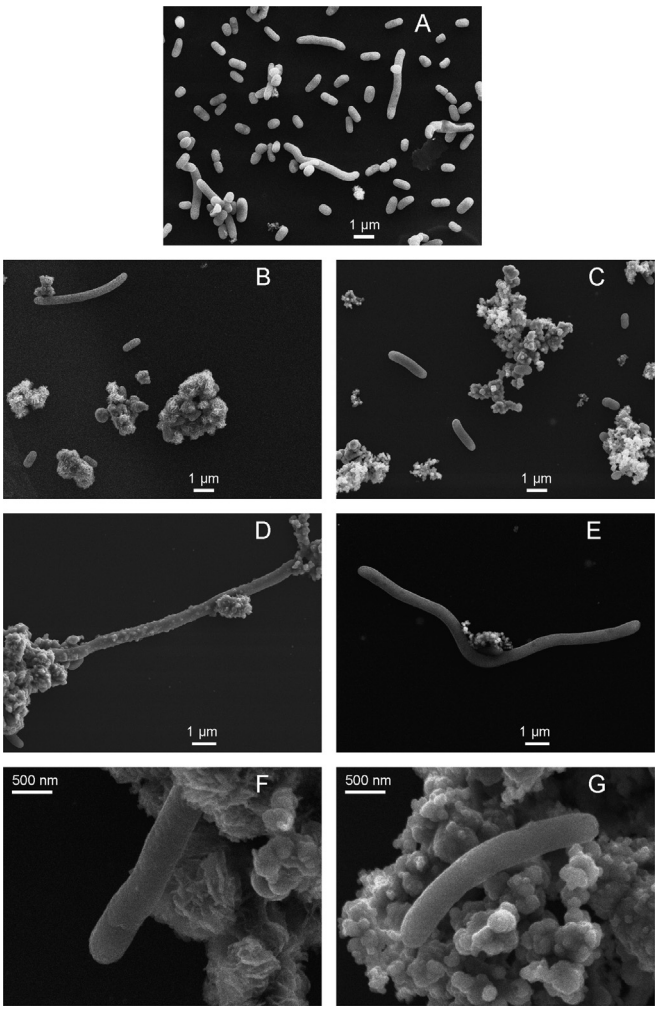

Fig. 3. FESEM images of the photoferrotrophic strain *Chlorobium ferrooxidans* KoFox in co-culture with the fermenting strain *Geospirillum* sp. KoFum grown with H_2 (A) or Fe(II) as electron donors, either in the absence (B, D, F) or presence (C, E, G) of 2 mM dissolved silica. Images D+E show elongated cells of strain KoFum. SE (5 kV).

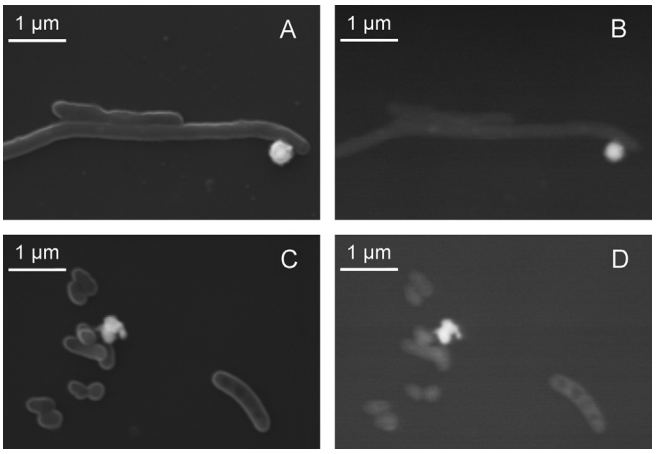

Fig. 4. SEM images of the photoferrotrophic strain *Chlorobium ferrooxidans* KoFox in co-culture with the fermenting strain *Geospirillum* sp. KoFum grown with Fe(II) as electron donor either in the absence (A, B) or presence (C, D) of 2 mM silica. SE (12 kV) (left) and BSE (12 kV) (right) images are shown to elucidate presence or absence of Fe minerals on the cell surfaces.

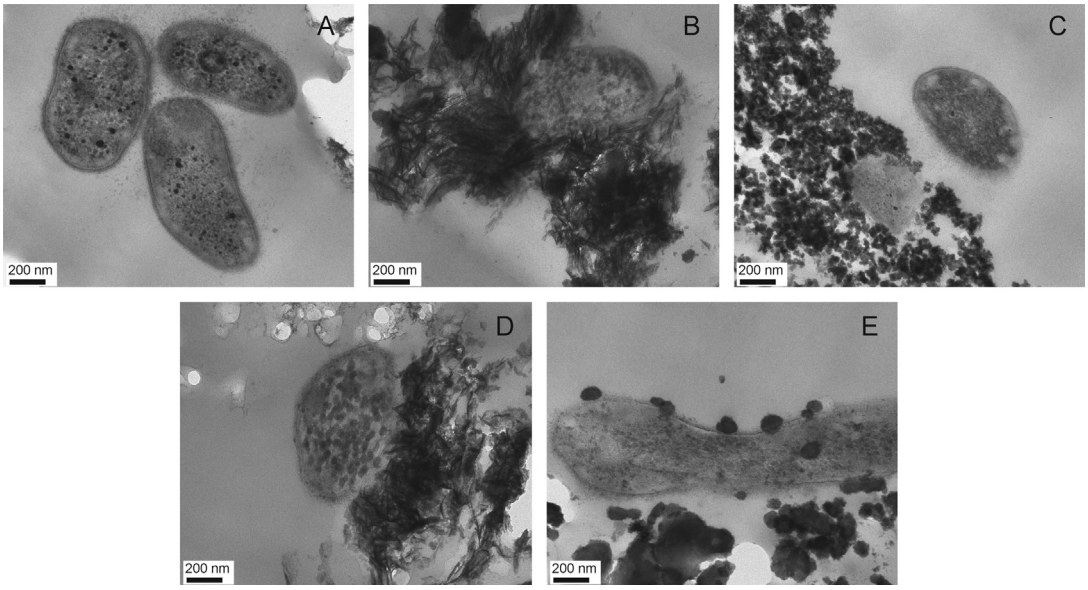

Fig. 5. TEM images of the photoferrotrophic strain *Chlorobium ferrooxidans* KoFox in co-culture with the fermenting strain *Geospirillum* sp. KoFum grown with either H_2 (A) or Fe(II) (B–E) as electron donor in the absence (B, D) or presence (C, E) of 2 mM dissolved silica. Samples were stained with osmium tetroxide and post-stained with uranyl acetate and lead citrate stain.

cells were associated with mineral aggregates (Fig. 5D) or with sparse mineral particles (Fig. 5E), but no distinct cell encrustation was observed.

3.3. Influence of silica and organics on mineralogy

Mineral analysis using µ-XRD showed that the mineral samples were predominantly X-ray amorphous and, therefore, most likely resemble the short range ordered mineral phase ferrihydrite, $Fe_{10}O_{14}(OH)_2$, simplified as $Fe(OH)_3$ (Wu et al., 2014), although one sample (Fig. 6B1) showed minor reflections corresponding to lepidocrocite, γ-FeO(OH), with broad reflections suggesting a small average crystallite size. Further analysis using Mössbauer spectroscopy supported this finding. The different mineral samples analyzed showed no obvious differences in spectra obtained at 77 K, with all of them having hyperfine parameters (Table 1) matching an octahedral Fe(III) mineral, such as ferrihydrite (Eickhoff et al., 2014). It is clear by looking at the hyperfine parameters that some differences occur, notably it appears that when silica is present (Fig. 6 B+D+F top), the samples show higher values of center shift (CS) but lower quadrupole splitting (QS) compared to samples with Si present. The QS is related to the asymmetry (i.e., non-sphericity) of the atom, hence the higher QS in samples prepared with Si suggests a greater degree of asymmetry caused by the substitution of Fe-atoms with Si-atoms (Eickhoff et al., 2014). Interestingly, these differences are most distinct in the presence of fumarate (Fig. 6 E+F top).

Fig. 6 and Table 1 show the fitting results for spectra measured at 5 K. The hyperfine fields (B_{hf}) determined through fitting are very low for all samples and are perhaps closer to that of lepidocrocite (Murad, 2010) which would agree with the results of µ-XRD for sample B1. However, based on the high CS and QS values recorded at 77 K, it is more likely that the mineral phase corresponds to ferrihydrite (Eickhoff et al., 2014). Nevertheless, it is clear that the mineral is a poorly crystalline Fe(III) phase in octahedral coordination. The spectra obtained at 5 K show that some samples were not fully magnetically ordered at this temperature, requiring an additional poorly crystalline sextet (denoted S2 in Table 1) for accurate fitting. This suggests a smaller particle size (Fig. 6 D–F) relative to the fully magnetically ordered samples (Fig. 6 A–C), especially in the presence of fumarate.

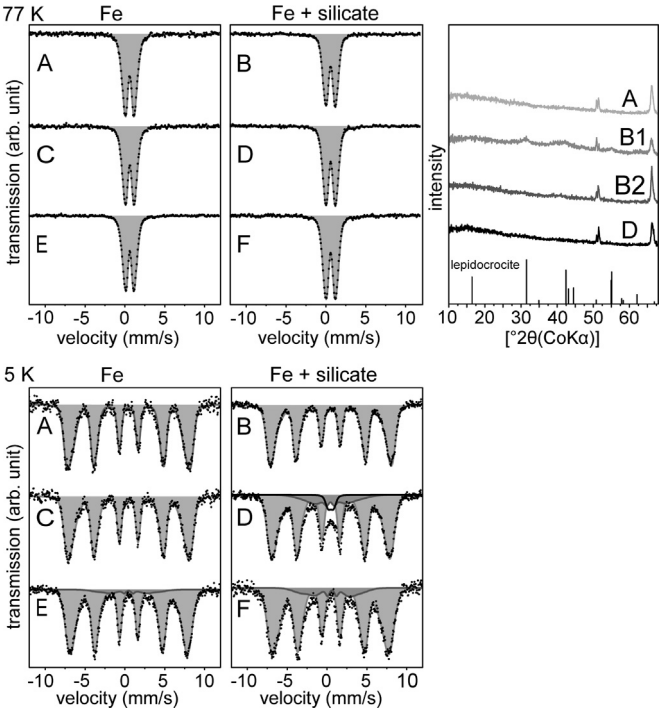

Fig. 6. ^{57}Fe Mössbauer spectra (left) and micro X-ray diffraction (µ-XRD) analysis (right) of mineral samples. Mössbauer spectra were measured at 77 K (top left) and 5 K (bottom left). Co-cultures of *Chlorobium ferrooxidans* KoFox and *Geospirillum* KoFum were cultivated at >1000 lux with ~3 mM Fe(II) (A) or ~3 mM Fe(II) and 2 mM dissolved silica (B), at 450 lux with ~3 mM Fe(II) (C), with ~3 mM Fe(II) and 2 mM dissolved silica (D), with ~3 mM Fe(II) and 5 mM fumarate (E) or with ~3 mM Fe(II), 2 mM dissolved silica and 5 mM fumarate (F). µ-XRD: signals at 51 and 66° 2θ values stem from the Si wafer that samples were mounted on.

The presence of silica only affected the crystallinity of some samples. While at high light conditions the spectra of samples taken from a co-culture grown in the presence or absence of silica were similar and showed no differences (Fig. 6 A+B top), samples taken from a co-culture grown at moderate light in the presence of silica showed a decrease in crystallinity as noted by the requirement for a partially collapsed sextet, in comparison to those

Table 1
Mössbauer hyperfine field parameters. Center shift (CS), quadrupole splitting (QS), hyperfine field (B_{hf}) and relative abundance (Pop.) of each phase corresponding to spectra measured at 5 K and 77 K. Db – doublet, S1 – well defined sextet, S2 – poorly defined sextet.

Sample	Temp. (K)	Phase	CS (mm/s)	QS (mm/s)	B_{hf} (T)	Pop. (%)	±
High light (A)	77	Db	0.48	0.83		100	N/A
	5	S1	0.486	−0.005	46.1	100	N/A
High light + Si (B)	77	Db	0.478	0.853		100	N/A
	5	S1	0.488	0.007	45.7	100	N/A
Normal light (C)	77	Db	0.484	0.816		100	N/A
	5	S1	0.488	−0.001	45.8	100	N/A
Normal light + Si (D)	77	Db	0.481	0.858		100	N/A
	5	Db	0.481	0.71		4.1	2.9
		S1	0.49	0.002	44.3	83.8	6.2
		S2	0.499	0.135	18.2	12.2	5.9
Normal light + Fum (E)	77	Db	0.485	0.791		100	N/A
	5	S1	0.487	0.018	44.6	94	3
		S2	0.464	0	21.7	6	3
Normal light + Fum + Si (F)	77	Db	0.481	0.861		100	N/A
	5	S1	0.489	−0.042	43.9	89.7	2.4
		S2	0.531	−0.192	21.8	10.3	2.4

samples formed in the absence of silica (Fig. 6 C+D). Such decreases in the crystallinity could be either due to a smaller average particle size, adsorption of Si that prevents formation of a perfect mineral crystal structure, or substitution of Si into the crystal structure.

4. Discussion

4.1. Impact of Si and organics on rates of Fe(II) oxidation

It was previously shown in cultures of nitrate-reducing, Fe(II)-oxidizing bacteria that higher concentrations of phosphate can decrease Fe(II) oxidation rates possibly due to formation of solid Fe(II)-phosphate phases that are more difficult to access as an iron source (Larese-Casanova et al., 2010). In our co-culture KoFox/KoFum, changes in the geochemical composition of the medium and the light intensities applied also influenced the Fe(II) oxidation rates, and thus obviously the activity of the phototrophic Fe(II)-oxidizer. We found that in the absence of dissolved silica, Fe(II) oxidation rates were highest at moderate light conditions, while high light conditions decreased the rates of phototrophic Fe(II) oxidation. In contrast, the addition of dissolved silica to our Fe(II)-oxidizing co-culture resulted in a higher tolerance towards higher light intensities, i.e., Fe(II) oxidation rates increased with higher light intensities and were highest under high light conditions.

The lower oxidation rates at high light intensity in the absence of Si are potentially a consequence of too much illumination and/or the toxic effects of high dissolved Fe(II) concentrations. Generally, it is expected that metabolic rates of phototrophs increase with increasing light intensity until a certain saturation level is reached. This was shown to be the case also for photoferrotrophs (Hegler et al., 2008). Toxic effects of Fe(II) are usually considered to be due to the formation of reactive oxygen species (ROS) via the O_2-dependent Fenton reaction which leads to oxidative damage of major biomolecules in cells. However, even under anoxic conditions the activity and growth of microorganisms can be reduced by high Fe(II) concentrations: For *Rhodobacter capsulatus* strain SB1003 it was shown that Fe(II) did inhibit growth in the presence of organics and particularly in the presence of humic substances potentially due to direct effects of the Fe(II) on metallo-enzymes of the cells (Poulain and Newman, 2009). In case of chemotrophic streptococci grown under anoxic conditions, Fe(II) did inhibit the F-ATPase, and thereby the cell's tolerance toward acidic conditions (Dunning et al., 1998). In a photic habitat, the Fe(II) toxicity might be in part due to O_2-independent photochemical reactions of Fe(II) that can also produce radicals in the form of ROS; for example, water molecules from O_2-free water can react with defective, nonstoichiometric Fe(III) sites of the Fe(II)-containing mineral pyrite (FeS_2), producing hydroxyl radicals, restoring Fe(II) and forming H_2O_2 (Borda et al., 2003). These reactions proceed in the dark, but are enhanced in the presence of visible light (Borda et al., 2003). Since in our experiments both organic matter (cell-derived biomolecules) and Fe(II)-bearing minerals (formed from the added Fe(II) with bicarbonate or phosphate present in the growth medium) are present, one could speculate that in our experiments the Fe(II) might have reacted as described above, to form radicals that could subsequently harm biomolecules in the cells and on the surface of cells.

The addition of dissolved silica likely protected the cells from these toxic effects caused by the combination of high light and high Fe(II) concentrations. This cell protection might be due to changes in Fe complexation and Fe speciation upon addition of silica. However, at circumneutral pH, quantitative information on the exact identity, stoichiometry and stability of such Fe–Si complexes is limited (Pokrovski et al., 2003). It is known that the presence of dissolved silica influences Fe(III) hydrolysis and precipitation, and it was shown that in presence of dissolved silica during abiotic Fe(II) oxidation, the Fe(III) colloids formed are stabilized (Mayer and Jarrell, 1996). In a previous study it was also suggested that silica remained largely in solution as monomeric silica in supernatants of photoferrotrophs during and after Fe(II) oxidation (Konhauser et al., 2007) despite its high affinity for Fe(III) (oxyhydr)oxides. Although the interpretation of the observed (toxic) effects of high light and Fe(II) on metabolic activity and the rescuing effects of Si remain mostly speculative at the moment, our data clearly shows that the activity of photoferrotrophs depends on these three parameters. Consequently, to fully evaluate the activity of these organisms on ancient Earth, these parameters need to be considered. It is also clear that for a mechanistic understanding of the effects of light, Si and Fe(II) concentrations on phototrophic Fe(II) oxidation, more studies are needed.

4.2. Impact of fumarate and silica on mineralogy

In the course of microbial Fe(II) oxidation, Fe(III) (oxy)hydroxides, such as ferrihydrite, goethite, lepidocrocite or magnetite form (Posth et al., 2014). Which Fe(III) minerals are precipitated in Fe(II)-oxidizing cultures, and their properties, depend on a variety of parameters, including (1) the composition and pH of the mineral medium, (2) Fe(II) oxidation rates, (3) the presence of mineral nucleation sites, (4) the presence of interfering ions (silica, organics, phosphate, etc.), and (5) potentially even the size and/or orientation of the incubation vessels (Dippon et al., 2012, 2015; Larese-Casanova et al., 2010; Posth et al., 2014). The presence of chloride in the medium favors the formation of lepidocrocite and higher concentrations of phosphate have been shown to favor poorly ordered ferrihydrite (or Fe(III) phosphate). The presence of humics or bicarbonate can lead to goethite precipitation (Larese-Casanova et al., 2010). Phosphate can influence Fe(II) oxidation rates (Larese-Casanova et al., 2010) and lower rates were shown to lead to production of more crystalline phases, e.g., goethite, in cultures of nitrate-reducing Fe(II)-oxidizers. Dissolved silica can also influence mineralogy in Fe(II)-oxidizing cultures and hinder mineral transformation from poorly crystalline to more crystalline Fe(III) oxyhydroxides (Eickhoff et al., 2014).

In our experiments, the addition of dissolved silica did not influence mineralogy, but it changed the morphology probably by

influencing the crystallization process. For instance, Fe(III) minerals produced by the KoFox/KoFum co-culture in the absence of silica had needle-like, spiky structures compared to more globular structures in the presence of silica. Such an influence of Si on mineral morphology was also observed in cultures of the nitrate-reducing Fe(II)-oxidizing *Acidovorax* sp. strain BoFeN1 (Picard et al., 2015b). The presence of the organic acid fumarate resulted in decreased crystallinity (smaller particle size) of the biogenic Fe(III) minerals. Previous Mössbauer studies revealed that organic matter present during ferrihydrite synthesis can lead to a decrease in magnetic ordering, hence smaller particle size (Mikutta et al., 2008). For the KoFox/KoFum co-culture it has been shown that KoFum metabolizes fumarate and produces other organic acids (Heising et al., 1999). Indeed, HPLC measurements of the supernatant of our cultures incubated with fumarate confirmed the presence of not only fumarate but also other organics (e.g., malate) that are produced by the co-culture during its metabolism (data not shown). This confirms that these organic compounds could have led to the changes in mineral properties observed.

Our experiments further showed that under all different growth conditions, including the presence or absence of dissolved silica, as well as changing light intensities, the precipitation of poorly crystalline mineral phases was favored. Using both μ-XRD and Mössbauer spectroscopy, we found only a minor influence of dissolved silica on the mineralogy of the biogenic minerals in this Fe(II)-oxidizing co-culture KoFox/KoFum, although the presence of silica would possibly influence subsequent diagenetic mineral transformation processes and prevent or slow down the transformation to more crystalline Fe mineral phases (Posth et al., 2013; Toner et al., 2012). Both silica and cell-derived organic molecules associated with the Fe(III) minerals appear to impact the long-term fate of the minerals deposited to the ancient ocean floor. On the one hand, it has been demonstrated that ferrihydrite associated with organic matter is more stable (less prone to thermal transformation to hematite) than ferrihydrite alone (Toner et al., 2012). On the other hand, it was shown in diagenesis simulation experiments that at higher temperatures (170 °C, 1.2 kbar) ferrihydrite alone was transformed to hematite, but in presence of glucose it was transformed to hematite, magnetite and siderite (Posth et al., 2013).

4.3. Cell–mineral aggregates and encrustation

In a previous study on cell–mineral aggregate formation by anaerobic Fe(II)-oxidizing bacteria, Schädler et al. (2009) used SEM to image the associations of KoFox with Fe(III) minerals. They detected sparse Fe particles on the cell surfaces, but no encrustation of the KoFox cells by the Fe(III) minerals produced. By contrast, those same authors detected that cells of the partner strain KoFum were encrusted in a thin layer of Fe(III) minerals. In our images, the KoFox/KoFum co-culture showed no distinct encrustation pattern under any of the tested conditions and neither strain showed encrustation as observed for strain KoFum by Schädler et al. (2009). Although we basically used the same sample preparation protocol as described in Schädler et al. (2009), slight differences in sample preparation (e.g., the HMDS treatment instead of critical point drying) might have influenced the outcome. Alternatively, the differences in cell encrustation observed might simply be due to the different cultures and the specific age of the samples analyzed; these were not identical in both studies.

The observation that neither the Fe(II)-oxidizing KoFox strain nor the co-partner strain KoFum encrusts in Fe(III) minerals raises the question of how these (presumably negatively charged) cells prevent the binding of Fe(III) ions and Fe(III) minerals to the cells? One possible explanation could be that for biogenic minerals produced by either phototrophic or chemotrophic Fe(II)-oxidizing bacteria an isoelectric point (iep) of 4.4 was determined compared to an iep of 8.8 for chemically synthesized ferrihydrite (F. Hegler and A. Kappler, unpublished data). This suggests that a negative charge on both the biogenic minerals and the cells prevented mineralization. Nevertheless, in some cultures of nitrate-reducing Fe(II)-oxidizing bacteria encrustation in biogenic Fe(III) minerals occurs, but obviously not in photoferrotrophic cultures (Schädler et al., 2009).

To prevent encrustation would be particularly crucial for pelagic phototrophic microorganisms since encrusted cells would sediment with the minerals, but as phototrophs these cells are dependent on remaining in the photic zone of the water column where they can perform photosynthesis. In contrast, benthic phototrophic communities are already at the shallow seafloor, and presumably encrustation only becomes an issue if they are not able to receive sufficient illumination. In the case of the phototrophic Fe(II)-oxidizing purple sulfur bacterium *Thiodictyon* sp. strain F4, it has been shown that the cells are able to lower the pH and establish a pH-microenvironment in close cell vicinity (Hegler et al., 2010). In combination with providing a mineral precipitation template in the form of organics, e.g., extracellular polymeric substances (EPS), this leads to Fe(III) mineral precipitation at a distance to the cell (Schädler et al., 2009). Furthermore, altering of the cell's surface properties was shown to facilitate targeted mineral precipitation in microaerophilic Fe(II)-oxidizing strains, thus preventing their complete encrustation (Saini and Chan, 2013). It was also suggested that partially Fe(III)-encrusted cells might be able to shed part of their mineralized cell surface (Emerson and Revsbech, 1994), something akin to what was shown a number of years ago with the cyanobacterium *Synechococcus* that is able to discard gypsum and calcite off its S-layers (Schultze-Lam et al., 1992). In addition, the complexation of Fe(III) by organic ligands produced by microorganisms can keep the Fe(III) in solution preventing precipitation, although this could constitute a costly investment for an autotrophic organism deriving its electrons from Fe(II) (Croal et al., 2004; Hegler et al., 2010). Whether one, or more, of these mechanisms is playing a role in the KoFox/KoFum co-culture to prevent encrustation needs to be further investigated.

4.4. Implications for ancient oceans, mineral and carbon deposition and fossil preservation

The production of poorly crystalline mineral phases, such as ferrihydrite, by the KoFox/KoFum co-culture is only weakly influenced by the presence of interfering ions. This suggests that such poorly crystalline mineral phases could have been the most dominant biologically produced minerals in the Precambrian oceans, even in the presence of high silica concentrations and at different light intensities associated with different depths in an ancient ocean water column. This correlates well with previous findings which suggested that poorly crystalline, amorphous Fe(III) mineral phases, e.g. ferrihydrite, were the main product of Fe(II) oxidation in Precambrian oceans (Kappler et al., 2005; Konhauser et al., 2005). Additionally, a recent study suggested that at pH 7.7–8.3 a hydrous Fe(II)-silicate gel could have precipitated in Precambrian oceans and have formed the mineral greenalite which is also found in BIF (Tosca et al., 2015). Although another recent study in a modern ferruginous lake suggested an important role of green rust in ancient environments (Zegeye et al., 2012), the influence of silica on green rust formation has not yet been determined, and as such, its potential role remains speculative (e.g., Konhauser et al., 2015).

When ferrihydrite is formed, it can lead to hematite formation via dehydration and to siderite and magnetite formation via microbial or thermochemical Fe(III) reduction (Konhauser et al., 2005; Posth et al., 2013). In case green rust is formed, this will more

likely lead to formation of lepidocrocite, goethite, or magnetite (Cornell and Schwertmann, 2003; Dippon et al., 2012). The formation of green rust also has implications for the fate of nutrients (such as phosphate) and trace metals (such as Ni) as their binding affinities to poorly crystalline Fe(III) mineral phases (such as ferrihydrite) and green rust are different. However, in order to evaluate whether green rust or rather poorly crystalline Fe(III) (oxy)hydroxides are relevant in these environments, a variety of parameters such as pH, salinity and temperature of ancient oceans should be taken into account. A difference in pH of ancient oceans has to be considered since the pH will influence the stability of ferrihydrite and green rust (Cornell and Schwertmann, 2003). Estimates of the pH in Precambrian oceans range from pH 6 to 8 and depend strongly on the assumed partial pressure of CO_2 in the early atmosphere, but might have been similar to our modern oceans (pH 8.1, Grotzinger and Kasting, 1993).

The rather loose cell–mineral associations observed for KoFox/KoFum will have consequences for the preservation of photoferrotrophic organisms into the rock record as compared to other Fe(II)-oxidizing organisms that form mineral crusts around the cells (Larese-Casanova et al., 2010; Schädler et al., 2009). For instance, it has been shown that the shape of microbial cells is well preserved after heating (600 °C for 20 h or 300 °C for 100 h) when these cells are encrusted in Fe(III) (oxyhydr)oxide minerals (Li et al., 2013), although earlier studies demonstrated the simple adsorption of Fe^{3+} was not sufficient to preserve the cell (Beveridge et al., 1983). Recently, diagenetic experiments demonstrated the preservation of encrusted nitrate-reducing Fe(II)-oxidizing bacteria and of twisted stalks (consisting of Fe(III) minerals and organics) produced by microaerophilic Fe(II)-oxidizing bacteria including the organic components suggesting that cells or extracellular structures associated with Fe minerals are more likely to be preserved (Picard et al., 2015a, 2015b). Indeed, microfossils of microaerophilic Fe(II)-oxidizing bacteria in the form of mineralized stalks and sheaths have been found in 490 Mio year old jaspers formed at marine hydrothermal vent sites (Little et al., 2004). In contrast, the loose cell–mineral associations in the KoFox/KoFum co-culture and other photoferrotrophic strains (Schädler et al., 2009; Wu et al., 2014), instead of cell encrustation or formation of stalks/sheaths, might therefore be one of the reasons that it is difficult to find such microfossils in BIF. Indeed, it has always been interesting that so few microfossils have been recovered from BIF. Previous explanations have assumed that the burial of ferric iron and organic biomass would have facilitated Fe(III) reduction and thus the complete oxidation of the carbon (e.g., Konhauser et al., 2005), although one might yet expect cellular outlines to be preserved. In that regard, the most documented examples of fossilized Fe(II)-oxidizing bacteria come from Paleoproterozoic samples (e.g., Planavsky et al., 2009; Schelble et al., 2004). However, many of the microfossils are actually preserved in chert and it has recently been argued that 'fossilization' took place during much later diagenesis, and as such, might not be indicative of primary Fe(II)-oxidizing bacteria (Shapiro and Konhauser, 2015). The lack of initial iron encrustations, as documented here, might also suggest that the lack of cellular preservation in BIF might simply be due to the fact that the plankton never were mineralized in the first place, and thus any loose association of iron minerals and biomass in the water column would have been destroyed during burial.

Finally, the presence or absence of a strong association of cells with minerals or encrustation in minerals also influences the rate and extent of sedimentation of the microbial cells, i.e., the biomass. Although fully encrusted cells with a high organic matter content will be lighter (have a lower density) than pure minerals or minerals only loosely associated with few cells (Posth et al., 2010), the sedimentation of encrusted cells will bring higher amounts of organics to the seafloor than cells with weaker associations to Fe(III) minerals or mineral-free cells that remain mostly suspended in the water column (Konhauser et al., 2005). Anoxygenic phototrophs incorporate 1 mol CO_2 into biomass with the oxidation of 4 mol Fe^{2+}. If all cells (the complete biomass) would sediment together with the produced Fe(III) minerals, this would lead to a Fe(III)/C_{org} ratio of 4:1 in the sediments. As Fe(III) re-reduction coupled to biomass mineralization requires the same ratio (4Fe(III):1C), this sedimentation could lead to total recycling of precipitated Fe(III). However, if no tight cell encrustation but the formation of more loose cell–mineral aggregates occurs (as observed in our case for KoFox/KoFum), less biomass attached to Fe(III) minerals would sink to the seafloor, lowering the ratio of Fe(III)/C_{org}, thus leading to an excess of Fe(III) in the bottom sediments (Konhauser et al., 2005). The implication is that during diagenesis and metamorphism, some of the Fe(III) sedimented could transform into hematite, with little to no organic carbon, while the co-delivery of biomass and ferric iron would serve to fuel sediment Fe(III) reduction that could lead to diagenetic magnetite and siderite formation; both the carbon-poor hematite and the Fe(II)-containing minerals a characteristic of BIF.

Taking all of these results into account, in combination with previous findings that GSB are possibly one of the most ancient photosynthetic organisms (Bryant and Liu, 2013), our findings on the one hand strengthen the importance of photoferrotrophs as a likely mechanism for BIF deposition on early Earth under predominantly anoxic conditions but, on the other hand, also suggest that preservation of remnants of Fe(II)-oxidizing GSB as microfossils in the rock record is unlikely.

Acknowledgements

This work was supported by the German Research Foundation (DFG) funded research training group RTG 1708 "Molecular principles of bacterial survival strategies" (to TG and AK) and by grant 165831 of the Natural Sciences and Engineering Research Council of Canada (NSERC) (to KOK). We would like to thank E. Struve for HPLC and M. Halama for µ-XRD measurements. F. Zeitvogel, P. Weigold and J. Harter are acknowledged for helpful discussions and A. Oatway for help with SEM and TEM work. We also thank G. Owttrim, D. Whitford, J. Havbeck and K. Semple for helpful assistance and use of their equipment.

References

Bekker, A., Planavsky, N.J., Krapež, B., Rasmussen, B., Hofmann, A., Slack, J.F., Rouxel, O.J., Konhauser, K.O., 2014. Iron formations: their origins and implications for ancient seawater chemistry. In: Holland, H.D., Turekian, K.K. (Eds.), Treatise on Geochemistry, 2 ed. Elsevier, Oxford, pp. 561–628.

Beveridge, T.J., Meloche, J.D., Fyfe, W.S., Murray, R.G.E., 1983. Diagenesis of metals chemically complexed to bacteria: laboratory formation of metal phosphates, sulfides, and organic condensates in artificial sediments. Appl. Environ. Microbiol. 45, 1094–1108.

Borda, M.J., Elsetinow, A.R., Strongin, D.R., Schoonen, M.A., 2003. A mechanism for the production of hydroxyl radical at surface defect sites on pyrite. Geochim. Cosmochim. Acta 67, 935–939.

Bryant, D.A., Liu, Z., 2013. Green bacteria: insights into green bacterial evolution through genomic analyses. In: Beatty, J.T. (Ed.), Advances in Botanical Research. Academic Press, pp. 99–150. Chapter four.

Cornell, R.M., Schwertmann, U., 2003. The Iron Oxides: Structure, Properties, Reactions, Occurences and Uses, 2 ed. Wiley–VCH Verlag GmbH & Co. KGaA, Weinheim.

Croal, L.R., Johnson, C.M., Beard, B.L., Newman, D.K., 2004. Iron isotope fractionation by Fe(II)-oxidizing photoautotrophic bacteria. Geochim. Cosmochim. Acta 68, 1227–1242.

Crowe, S.A., Jones, C., Katsev, S., Magen, C., O'Neill, A.H., Sturm, A., Canfield, D.E., Haffner, G.D., Mucci, A., Sundby, B., Fowle, D.A., 2008. Photoferrotrophs thrive in an Archean Ocean analogue. Proc. Natl. Acad. Sci. USA 105, 15938–15943.

Czaja, A.D., Johnson, C.M., Beard, B.L., Roden, E.E., Li, W., Moorbath, S., 2013. Biological Fe oxidation controlled deposition of banded iron formation in the ca.

3770 Ma Isua Supracrustal Belt (West Greenland). Earth Planet. Sci. Lett. 363, 192–203.
Dippon, U., Pantke, C., Porsch, K., Larese-Casanova, P., Kappler, A., 2012. Potential function of added minerals as nucleation sites and effect of humic substances on mineral formation by the nitrate-reducing Fe(II)-oxidizer *Acidovorax* sp. BoFeN1. Environ. Sci. Technol. 46, 6556–6565.
Dippon, U., Schmidt, C., Behrens, S., Kappler, A., 2015. Secondary mineral formation during ferrihydrite reduction by *Shewanella oneidensis* MR-1 depends on incubation vessel orientation and resulting gradients of cells, Fe^{2+} and Fe minerals. Geomicrobiol. J. 32, 878–889.
Dunning, J.C., Ma, Y., Marquis, R.E., 1998. Anaerobic killing of oral *Streptococci* by reduced, transition metal cations. Appl. Environ. Microbiol. 64, 27–33.
Eickhoff, M., Obst, M., Schröder, C., Hitchcock, A.P., Tyliszczak, T., Martinez, R.E., Robbins, L.J., Konhauser, K.O., Kappler, A., 2014. Nickel partitioning in biogenic and abiogenic ferrihydrite: the influence of silica and implications for ancient environments. Geochim. Cosmochim. Acta 140, 65–79.
Emerson, D., Revsbech, N.P., 1994. Investigation of an iron-oxidizing microbial mat community located near Aarhus, Denmark – field studies. Appl. Environ. Microbiol. 60, 4022–4031.
Grotzinger, J.P., Kasting, J.F., 1993. New constraints on Precambrian ocean composition. J. Geol., 235–243.
Hegler, F., Posth, N.R., Jiang, J., Kappler, A., 2008. Physiology of phototrophic iron(II)-oxidizing bacteria: implications for modern and ancient environments. FEMS Microbiol. Ecol. 66, 250–260.
Hegler, F., Schmidt, C., Schwarz, H., Kappler, A., 2010. Does a low-pH microenvironment around phototrophic Fe(II)-oxidizing bacteria prevent cell encrustation by Fe(III) minerals? FEMS Microbiol. Ecol. 74, 592–600.
Heising, S., Richter, L., Ludwig, W., Schink, B., 1999. *Chlorobium ferrooxidans* sp. nov., a phototrophic green sulfur bacterium that oxidizes ferrous iron in coculture with a "*Geospirillum*" sp. strain. Arch. Microbiol. 172, 116–124.
Holland, H.D., 1973. The oceans; a possible source of iron in iron-formations. Econ. Geol. 68, 1169–1172.
Jerlov, N.G., 1976. Marine Optics, 2, rev. and enl. ed. Elsevier, Amsterdam [u.a].
Jones, C., Nomosatryo, S., Crowe, S., Bjerrum, C., Canfield, D., 2015. Iron oxides, divalent cations, silica, and the early earth phosphorus crisis. Geology 43, 135–138.
Kappler, A., Pasquero, C., Konhauser, K.O., Newman, D.K., 2005. Deposition of banded iron formations by anoxygenic phototrophic Fe(II)-oxidizing bacteria. Geology 33, 865–868.
Konhauser, K.O., Amskold, L., Lalonde, S.V., Posth, N.R., Kappler, A., Anbar, A., 2007. Decoupling photochemical Fe(II) oxidation from shallow-water BIF deposition. Earth Planet. Sci. Lett. 258, 87–100.
Konhauser, K.O., Newman, D.K., Kappler, A., 2005. The potential significance of microbial Fe(III) reduction during deposition of Precambrian banded iron formations. Geobiology 3, 167–177.
Konhauser, K.O., Robbins, L.J., Pecoits, E., Peacock, C., Kappler, A., Lalonde, S.V., 2015. The Archean nickel famine revisited. Astrobiology 15, 804–815.
Lagarec, K., Rancourt, D.G., 1997. Extended Voigt-based analytic lineshape method for determining *N*-dimensional correlated hyperfine parameter distributions in Mössbauer spectroscopy. Nucl. Instrum. Methods Phys. Res., Sect. B, Beam Interact. Mater. Atoms 129, 266–280.
Larese-Casanova, P., Haderlein, S.B., Kappler, A., 2010. Biomineralization of lepidocrocite and goethite by nitrate-reducing Fe(II)-oxidizing bacteria: effect of pH, bicarbonate, phosphate, and humic acids. Geochim. Cosmochim. Acta 74, 3721–3734.
Li, J., Benzerara, K., Bernard, S., Beyssac, O., 2013. The link between biomineralization and fossilization of bacteria: insights from field and experimental studies. Chem. Geol. 359, 49–69.
Little, C.T.S., Glynn, S.E.J., Mills, R.A., 2004. Four-hundred-and-ninety-million-year record of bacteriogenic iron oxide precipitation at sea-floor hydrothermal vents. Geomicrobiol. J. 21, 415–429.
Llirós, M., García-Armisen, T., Darchambeau, F., Morana, C., Triadó-Margarit, X., Inceoğlu, Ö., Borrego, C.M., Bouillon, S., Servais, P., Borges, A.V., Descy, J.-P., Canfield, D.E., Crowe, S.A., 2015. Pelagic photoferrotrophy and iron cycling in a modern ferruginous basin. Sci. Rep. 5, 13803.
Mayer, T.D., Jarrell, W.M., 1996. Formation and stability of iron(II) oxidation products under natural concentrations of dissolved silica. Water Res. 30, 1208–1214.
Mikutta, C., Mikutta, R., Bonneville, S., Wagner, F., Voegelin, A., Christl, I., Kretzschmar, R., 2008. Synthetic coprecipitates of exopolysaccharides and ferrihydrite. Part I: Characterization. Geochim. Cosmochim. Acta 72, 1111–1127.
Morris, R.C., 1993. Genetic modelling for banded iron-formation of the Hamersley Group, Pilbara Craton, Western Australia. Precambrian Res. 60, 243–286.
Murad, E., 2010. Mössbauer spectroscopy of clays, soils and their mineral constituents. Clay Miner. 45, 413–430.
Picard, A., Kappler, A., Schmid, G., Quaroni, L., Obst, M., 2015a. Experimental diagenesis of organo–mineral structures formed by microaerophilic Fe(II)-oxidizing bacteria. Nat. Commun. 6, 6277.
Picard, A., Obst, M., Schmid, G., Zeitvogel, F., Kappler, A., 2015b. Limited influence of Si on the preservation of Fe-mineral encrusted cells during experimental diagenesis. Geobiology. http://dx.doi.org/10.1111/gbi.12171. In press.
Planavsky, N., Rouxel, O., Bekker, A., Shapiro, R., Fralick, P., Knudsen, A., 2009. Iron-oxidizing microbial ecosystems thrived in late Paleoproterozoic redox-stratified oceans. Earth Planet. Sci. Lett. 286, 230–242.
Pokrovski, G.S., Schott, J., Farges, F., Hazemann, J.-L., 2003. Iron (III)–silica interactions in aqueous solution: insights from X-ray absorption fine structure spectroscopy. Geochim. Cosmochim. Acta 67, 3559–3573.
Posth, N.R., Canfield, D.E., Kappler, A., 2014. Biogenic Fe(III) minerals: from formation to diagenesis and preservation in the rock record. Earth-Sci. Rev. 135, 103–121.
Posth, N.R., Huelin, S., Konhauser, K.O., Kappler, A., 2010. Size, density and composition of cell–mineral aggregates formed during anoxygenic phototrophic Fe(II) oxidation: impact on modern and ancient environments. Geochim. Cosmochim. Acta 74, 3476–3493.
Posth, N.R., Köhler, I.D., Swanner, E., Schröder, C., Wellmann, E., Binder, B., Konhauser, K.O., Neumann, U., Berthold, C., Nowak, M., Kappler, A., 2013. Simulating Precambrian banded iron formation diagenesis. Chem. Geol. 362, 66–73.
Poulain, A.J., Newman, D.K., 2009. *Rhodobacter capsulatus* catalyzes light-dependent Fe(II) oxidation under anaerobic conditions as a potential detoxification mechanism. Appl. Environ. Microbiol. 75, 6639–6646.
Saini, G., Chan, C.S., 2013. Near-neutral surface charge and hydrophilicity prevent mineral encrustation of Fe-oxidizing micro-organisms. Geobiology 11, 191–200.
Schädler, S., Burkhardt, C., Hegler, F., Straub, K.L., Miot, J., Benzerara, K., Kappler, A., 2009. Formation of cell–iron–mineral aggregates by phototrophic and nitrate-reducing anaerobic Fe(II)-oxidizing bacteria. Geomicrobiol. J. 26, 93–103.
Schelble, R.T., Westall, F., Allen, C.C., 2004. ~1.8 Ga iron-mineralized microbiota from the Gunflint Iron Formation, Ontario, Canada: implications for Mars. Adv. Space Res. 33, 1268–1273.
Schultze-Lam, S., Harauz, G., Beveridge, T.J., 1992. Participation of a cyanobacterial S layer in fine-grain mineral formation. J. Bacteriol. 174, 7971–7981.
Shapiro, R.S., Konhauser, K.O., 2015. Hematite-coated microfossils: primary ecological fingerprint or taphonomic oddity of the Paleoproterozoic? Geobiology 13, 209–224.
Siever, R., 1962. Silica solubility, 0°–200 °C, and the diagenesis of siliceous sediments. J. Geol. 70, 127–150.
Toner, B.M., Berquo, T.S., Michel, F.M., Sorensen, J.V., Templeton, A.S., Edwards, K.J., 2012. Mineralogy of iron microbial mats from Loihi Seamount. Front. Microbiol. 3, 118.
Tosca, N.J., Guggenheim, S., Pufahl, P.K., 2015. An authigenic origin for Precambrian greenalite: implications for iron formation and the chemistry of ancient seawater. Geol. Soc. Am. Bull. http://dx.doi.org/10.1130/B31339.1.
Widdel, F., Schnell, S., Heising, S., Ehrenreich, A., Assmus, B., Schink, B., 1993. Ferrous iron oxidation by anoxygenic phototrophic bacteria. Nature 362, 834–836.
Wu, W., Swanner, E.D., Hao, L., Zeitvogel, F., Obst, M., Pan, Y., Kappler, A., 2014. Characterization of the physiology and cell–mineral interactions of the marine anoxygenic phototrophic Fe(II) oxidizer *Rhodovulum iodosum* – implications for Precambrian Fe(II) oxidation. FEMS Microbiol. Ecol. 88, 503–515.
Zegeye, A., Bonneville, S., Benning, L.G., Sturm, A., Fowle, D.A., Jones, C., Canfield, D.E., Ruby, C., MacLean, L.C., Nomosatryo, S., Crowe, S.A., Poulton, S.W., 2012. Green rust formation controls nutrient availability in a ferruginous water column. Geology 40, 599–602.